A&A 471, 775–786 (2007)
DOI: 10.1051/0004-6361:20066708

Astronomy & Astrophysics

An XMM-*Newton* study of hyper-luminous infrared galaxies⋆

A. Ruiz, F. J. Carrera, and F. Panessa

Instituto de Física de Cantabria (IFCA), CSIC-UC, Santander 39005, Spain
e-mail: ruizca@ifca.unican.es

Received 7 November 2006 / Accepted 18 May 2007

ABSTRACT

Aims. Hyper-Luminous Infrared Galaxies (HLIRGs) are the most luminous persistent objects in the Universe. They exhibit extremely high star formation rates, and most of them seem to harbor an Active Galactic Nucleus (AGN). They are unique laboratories to investigate ultimate star formation, and its connection to super-massive black hole growth. X-ray studies of HLIRGs have the potential to unravel the AGN contribution to the bolometric output from these bright objects.
Methods. We have selected a sample of 14 HLIRGs observed by XMM-*Newton* (type 1, type 2 AGN and starburst), 5 of which are candidates to be Compton-thick objects. This is the first time that a systematic study of this type of objects has been carried out in the X-ray spectral band. Their X-ray spectral properties have been correlated with their infrared luminosities, estimated by *IRAS*, *ISO* and sub-millimeter observations.
Results. The X-ray spectra of HLIRGs present heterogeneous properties. All our X-ray detected HLIRGs (10) have AGN-dominated X-ray spectra. The hard X-ray luminosity of 8 of them is consistent with a pure AGN contribution, while in the remaining 2 sources, both an AGN and a starburst seem to contribute to the overall emission. We found soft excess emission in 5 sources. In one of them it is consistent with a pure starburst origin, while in the other 4 sources it is consistent with an AGN origin. The observed X-ray emission is systematically below that expected for a standard local QSO of the same IR luminosity, suggesting the possible presence of absorption in type 2 objects and/or a departure from a standard spectral energy distribution of QSO. The X-ray-to-IR-luminosity ratio is constant with redshift, indicating similar evolutions for the AGN and starburst component, and that their respective power sources could be physically related.

Key words. galaxies: active – galaxies: starburst – galaxies: evolution – X-rays: galaxies – infrared: galaxies

1. Introduction

Ultra-luminous Infrared Galaxies (ULIRGs) are a class of galaxies with bolometric luminosity $L_{\rm IR} \geq 10^{12}\ L_{\odot}$, dominated by the emission in the infrared (IR) waveband (see Sanders & Mirabel 1996, for a complete review). They are, together with optical quasars, the most luminous objects in the Local Universe. ULIRGs are rare in the Local Universe (Soifer et al. 1987), but large numbers are detected instead in deep-IR surveys, and are a fundamental constituent of the high redshift galaxy population (Smail et al. 1997; Genzel & Cesarsky 2000; Franceschini et al. 2001). They are powered by Active Galactic Nucleus (AGN) and/or starburst (SB) triggered by mergers of gas-rich spiral galaxies (Veilleux et al. 2002). Optical spectroscopic studies reveal that the fraction of ULIRGs hosting an AGN increases with increasing IR luminosity (Veilleux et al. 1995, 1999). Furthermore, the fraction of Seyfert 1 to Seyfert 2 ULIRGs increases with IR luminosity.

It has been proposed that ULIRGs at high redshift could be the origin of massive elliptical and S0 galaxies (Franceschini et al. 1994; Lilly et al. 1999; Genzel & Cesarsky 2000). A large fraction of stars in present day galaxies would have been formed during these evolutionary phases.

Observations in the X-ray band are a powerful tool to disentangle the AGN contribution to the bolometric luminosity from the ULIRGs. X-rays studies of ULIRGs have confirmed their composite nature (powered by AGN and/or starburst), with indications for a predominance of the SB over the AGN phenomenon, even when observed in hard X-rays (Franceschini et al. 2003).

The brightest end of the ULIRG distribution is occupied by the Hyper-Luminous Infrared Galaxies (HLIRGs, $L_{\rm IR} \geq 10^{13}\ L_{\odot}$). These are among the most luminous objects in the Universe, although the origin of this luminosity is still uncertain. This population exhibits extremely high star formation rates (SFR), and most seem also to harbor an AGN (Rowan-Robinson 2000).

The source and trigger of the emission from HLIRGs have been discussed since their discovery. Initially the extreme luminosity of HLIRGs was attributed to gravitational magnification, but *Hubble Space Telescope* (*HST*) observations discovered that only a minority of these galaxies (∼15–20%) have been misclassified owing to lensing (Farrah et al. 2002b). Currently, there are three main hypotheses on the nature of these objects:

a) they could be simply the high luminosity tail of the ULIRG population, and therefore their power sources are probably triggered by galaxy mergers. Though *HST* has revealed some merging systems among HLIRGs, there is a significant fraction of them in isolated systems (Farrah et al. 2002b);
b) assuming that the majority of the rest-frame far infrared (FIR) and sub-millimeter (sub-mm) emission comes from star formation (Verma et al. 2002; Farrah et al. 2002a), their estimated SFR are >1000 $M_{\odot}\,{\rm yr}^{-1}$, the highest for any object in the Universe. HLIRGs could be very young galaxies going through their major episode of star formation (Rowan-Robinson 2000);

⋆ Figure 1 is only available in electronic form at
http://www.aanda.org

c) they may be a completely new class of objects, where the IR emission is originated via some other mechanism: e.g., a transient IR-luminous phase in quasar evolution (Farrah et al. 2002b).

The state-of-the-art X-ray, IR and sub-mm observations suggest that HLIRGs are powered by dust-enshrouded black hole accretion and violent star formation (Rowan-Robinson 2000; Verma et al. 2002; Farrah et al. 2002a; Wilman et al. 2003; Iwasawa et al. 2005), pointing to a mixture of the (a) and (b) hypotheses. Recent observations of individual HLIRGs with *Chandra* and XMM-*Newton* show that the IR emission of these objects could be powered by buried quasars through dust re-radiation. The nuclear source is heavily obscured, reaching the Compton-thick (CT) limit (Iwasawa et al. 2001; Wilman et al. 2003; Iwasawa et al. 2005). It has also been suggested that galaxy mergers in an over-density region may be a necessary condition for the formation of this class of sources (Iwasawa et al. 2005). However this suggestion is in contradiction with the significant fraction of isolated HLIRGs found by Farrah et al. (2002b).

AGN research has taken a central role in the study of galaxy formation and evolution since the discovery that most local spheroidal galaxy components (elliptical galaxies and the bulge of spiral galaxies) contain a super-massive black hole with the mass being proportional to the stellar mass of the galaxy spheroid (Magorrian et al. 1998; McLure & Dunlop 2002).

These facts are most easily explained if the formation of the super-massive black hole and the spheroid of galaxies were coeval, i.e., the black hole was built up by accretion of the same gas that rapidly formed the stars of the spheroid (Page et al. 2004; Di Matteo et al. 2005).

Additional evidence for the coeval hypothesis is the similarity between the evolution of cosmic star formation and luminous AGN activity, since both were much higher in the past up to redshift ∼2, than in the present day (Franceschini et al. 1999; Silverman et al. 2005). As HLIRGs could represent the most vigorous stage of galaxy formation, they are unique laboratories to investigate extremely high stellar formation, and its connection to super-massive black hole growth.

The main objective of this paper is to determine the relative contribution of SB and AGN emission to the bolometric luminosity in HLIRGs, and the interplay between those two phenomena, as well as how their relative contribution varies with cosmic time. In our study we have also compared the properties of HLIRGs to those of ULIRGs.

We have used X-ray observations of HLIRGs from XMM-*Newton* and also public data from the *Chandra* archive. In Sect. 2 the sample selection is explained. Data reduction and spectral analysis of each source are described in Sect. 3. Results are discussed in Sect. 4. Section 5 summarizes our conclusions.

The *Wilkinson Microwave Anisotropy Probe* (*WMAP*) concordance cosmology has been adopted in the paper: $H_0 = 70\ \mathrm{km\,s^{-1}\,Mpc^{-1}}$, $\Omega_\mathrm{m} = 0.27, \Omega_\Lambda = 0.73$ (Spergel et al. 2003).

2. The HLIRG sample

Our sample of HLIRGs has been selected from the Rowan-Robinson (2000) sample of 45 HLIRGs. The sources in this mother sample can be classified in four sub-samples: (1) objects found from direct optical follow-up of 60 μm or 850 μm surveys; (2) sources found from comparison of known quasar and radio galaxy lists with 60 μm catalogues, or using IR color selection (biased to AGN); (3) sources selected from sub-mm observations of known high-redshift AGN; and (4) known luminous IR galaxies not included in the previous subsamples, but satisfying $L_\mathrm{IR} > 10^{13}\ L_\odot$. The first one is a flux-limited sample, unbiased towards AGN; the sources in the second and third sub-samples have been selected in order to host an AGN, and therefore suffer from selection effects.

We chose those HLIRGs from the Rowan-Robinson (2000) sample with public data available in the XMM-*Newton* Science Archive (XSA), as of December 2004. We also included observations of five sources from OBS-ID 030536 by our group (see Table 2). We then constrained the resulting sample to those sources with redshift less than ∼2, to prevent a strong bias due to the presence of high-z QSOs. In our final sample there are 8 sources which are included in the first Rowan-Robinson (2000) subsample, 4 sources are in the second subsample, 1 source is in the third and 1 is in the fourth one. Most of our sources are selected from subsamples which are in principle not biased in favor of AGN. However, selecting the sample by using the availability of XMM-*Newton* data probably introduces a selection effect in favor of the presence of an AGN. Moreover, estimating the completeness level of this sample is difficult, since it is not flux limited. From IR and sub-mm unbiased surveys, Rowan-Robinson (2000) estimates that the number of HLIRGs brighter than 200 mJy at 60 μm over the whole sky is 100–200. 14 of them are included in our sample, which is the largest sample of HLIRGs studied in X-rays.

Table 1 describes our sample. Column 2 shows the optical spectral classification as derived from the literature: twelve sources in our sample present AGN characteristics. Eight of them are classified as "type 1", and four of them as "type 2". We have classified QSO instead of Seyfert to those objects with intrinsic 2–10 keV luminosity $>10^{44}$ erg s^{-1} (see Table 4). A couple of sources have been classified from the literature as "Narrow line" (NL) sources, i.e. which show narrow forbidden emission lines typical of HII regions. All "type 2" and one NL-SB galaxy are CT candidates.

The analysis of the IR Spectral Energy Distribution (SED) of our sources has revealed that the SED can be modeled by a combination of an AGN and a SB components (Rowan-Robinson 2000; Verma et al. 2002; Farrah et al. 2002a). In Table 1, Col. 3 we report the fraction of the AGN and SB component needed to fit the SED. Three objects are completely dominated by the AGN component, while in other three the SB component is dominant.

In order to compare the properties of HLIRGs with other similar classes of objects, we have included two samples in our study. We chose a sample of 10 ULIRGs studied in X-rays by XMM-*Newton* (Franceschini et al. 2003). The sample is flux-limited at 60 μm and complete to $S_{60\,\mu\mathrm{m}} \geq 5.4$ Jy. In addition, we have selected all the HLIRGs (six) from the Stevens et al. (2005) sample of high redshift X-ray Compton-thin absorbed QSO. These sources have been observed in X-rays by *ROSAT* (Page et al. 2001) and by XMM-*Newton* (Page et al. 2007), and by SCUBA in the sub-mm band (Page et al. 2004).

3. X-ray data reduction and analysis

3.1. Data reduction

Table 2 presents the most relevant information about the XMM-*Newton* observations. The data have been processed using the Science Analysis System (SAS) version 6.1.0, and have been analyzed using the standard software packages (FTOOLS and XSPEC) included in HEAsoft 5.3.1.

We reprocessed the EPIC PN and MOS Observation Data Files (ODFs) to obtain new calibrated and concatenated event

Table 1. Hyper-luminous galaxies observed by XMM-*Newton* with redshift less than ∼2.

Source	Type[a]	IR-Model[b] AGN / SB		RA	Dec	z	$L_{\rm FIR}$ [erg s^{-1} cm^{-2}]
IRAS 00182-7112	QSO 2 (CT)	0.35 / **0.65**	RR00	00 20 34.7	–70 55 27	0.327	46.49
IRAS F00235+1024	NL SB (CT)	0.5 / 0.5	F02a	00 26 06.5	+10 41 32	0.575	<46.76
IRAS 07380-2342	NL	**0.6** / 0.4	F02a	07 40 09.8	–23 49 58	0.292	46.56
IRAS 09104+4109[c]	QSO 2 (CT), cD	**1** / 0	RR00	09 13 45.4	+40 56 28	0.442	<46.42
PG 1206+459	QSO	**1** / 0	RR00	12 08 58.0	+45 40 36	1.158	47.20
PG 1247+267	QSO	**1** / 0	RR00	12 50 05.7	+26 31 08	2.038	47.70
IRAS F12509+3122	QSO	**0.6** / 0.4	F02a	12 53 17.6	+31 05 50	0.780	<46.86
IRAS 12514+1027	Sy2 (CT)	0.4 / **0.6**	RR00	12 54 00.8	+10 11 12	0.3	46.18
IRAS 13279+3401	QSO[d]	**0.7** / 0.3	F02a	13 30 15.3	+33 46 29	0.36	46.58
IRAS 14026+4341	QSO 1.5[d]	**0.6** / 0.4	F02a	14 04 38.8	+43 27 07	0.323	46.26
IRAS F14218+3845	QSO	0.2 / **0.8**	F02a	14 23 55.0	+38 32 14	1.21	47.80
IRAS F15307+3252	QSO 2 (CT)	**0.7** / 0.3	V02	15 32 44.0	+32 42 47	0.926	<47.07
IRAS 16347+7037	QSO	**0.8** / 0.2	F02b	16 34 28.9	+70 31 33	1.334	47.42
IRAS 18216+6418[c]	QSO 1.2, cD	**0.6** / 0.4	F02a	18 21 57.3	+64 20 36	0.297	46.49

[a] NL: narrow-line objects; Sy2: Seyfert 2. Compton-thick candidates are labeled as CT. Spectral classification from Rowan-Robinson (2000), except IRAS F00235+1024 (Verma et al. 2002), IRAS 14026+4321 (Wang et al. 2006) and IRAS 18216+6418 (Véron-Cetty & Véron 2006). IRAS 00182-7112 has been classified as type 2 source using the optical emission lines from Armus et al. (1989) and the diagnostic diagrams from Osterbrock (1989, chap. 12). [b] Fraction of the IR emission originating in AGN and/or SB. See Sect. 2 for details. Data from: (RR00) Rowan-Robinson (2000), (F02a) Farrah et al. (2002a), (V02) Verma et al. (2002), (F02b) Farrah et al. (2002b). [c] Source in cluster. [d] Not detected in X-rays. We use the optical data to classify this source as QSO. See Sect. 2 for details.

Table 2. XMM-*Newton* observations description.

Source	Net. exp. time [ks]			Ext. radius [arcsec]			Source counts[a]			Obs. date	Filter
	PN	MOS1	MOS2	PN	MOS1	MOS2	PN	MOS1	MOS2		
IRAS 00182-7112	9.1	–	–	19	–	–	134 ± 15	–	–	2003-04-17	Thin
IRAS F00235+1024	14.4	–	–	35	–	–	<30	–	–	2001-01-10	Thin
IRAS 07380-2342	4.7	11.4	11.6	30	40	40	<45	–	–	2005-10-13[c]	Medium
IRAS 09104+4109[b]	9.2	12.6	12.5	20	20	20	5544 ± 75	2245 ± 47	2332 ± 48	2003-04-27	Medium
PG 1206+459	5.9	6.9	6.9	26	32	29	731 ± 32	188 ± 16	193 ± 16	2002-05-11	Thin
PG 1247+267	19.4	25.5	26.6	35	35	35	5132 ± 74	1646 ± 42	1694 ± 43	2003-06-18	Medium
IRAS F12509+3122	11.9	14.6	14.1	25	25	25	508 ± 24	156 ± 13	139 ± 13	2005-12-11[c]	Thin
IRAS 12514+1027	16.7	20.0	18.2	22	40	40	105 ± 22	28 ± 13	7 ± 12	2001-12-28	Thin
IRAS 13279+3401	24.6	–	–	25	–	–	<36	–	–	2006-01-18[c]	Medium
IRAS 14026+4341	–	6.6	5.6	–	35	35	–	<30	<27	2005-11-26[c]	Thin
IRAS F14218+3845	11.5	15.2	15.1	30	34	31	550 ± 29	185 ± 17	176 ± 16	2003-08-01	Medium
	2.3	7.3	7.0	30	30	30	91 ± 14	109 ± 20	79 ± 18	2005-06-07[c]	Medium
IRAS F15307+3252	9.4	11.5	12.0	22	40	40	97 ± 21	30 ± 12	42 ± 13	2002-07-30	Medium
IRAS 16347+7037	12.9	15.6	15.8	30	56	48	11172 ± 106	3546 ± 67	3785 ± 66	2002-11-23	Medium
IRAS 18216+6418[b]	0.5	2.9	3.3	20	20	20	–	7402 ± 86	8481 ± 92	2002-10-16	Thin

[a] Total source counts in the 0.2–10 keV band. [b] *Chandra* data are also used in the study of this source. See Sect. 3.3 for details. [c] Data from OBS-ID 030536.

lists, using the SAS tasks `EMPROC` and `EPPROC`, including the latest calibration files at the time of reprocessing.

The new event files were filtered to avoid intervals of flaring particle background, and only events corresponding to pattern 0–12 for MOS and 0–4 for PN were used (Ehle et al. 2005). The events with energy above 12 keV and below 0.2 keV were also filtered out. The source spectra were extracted from circular regions, whose radii were chosen in each case to optimize the signal-to-noise ratio (S/N), and to avoid the CCD gaps. The background spectra were taken in circular source-free regions near the object, also avoiding CCD gaps. We generated our own redistribution matrices and ancillary files (correction for the effective area) using the SAS tasks `RMFGEN` and `ARFGEN`.

XMM-*Newton* has detected 10 out of 14 sources (∼70%) with different S/N quality. In cases where the S/N ratio was poor, the MOS and PN spectra were co-added (Page et al. 2003). All spectra were rebinned to have ≥25 counts per energy channel, except IRAS 00182-7112 (≥15 counts) and PG 1206+459 (≥20 counts). The resulting EPIC spectra (see Fig. 1) reveal heterogeneous spectral properties for these objects (see Table 4 and Sects. 3.4, 3.5).

3.2. Non-detected sources

We have estimated upper limits to the luminosity of the sources not detected by XMM-*Newton*. We estimated the count rate which would correspond to 3σ fluctuations of the background in a circular region of the PN-EPIC images, centered in the source coordinates. To convert between count rate and physical units a simple model was chosen: a power law with $\Gamma = 2$ and Galactic absorption.

3.3. Cluster emission subtraction

Two sources of our sample, IRAS 09104+4109 and IRAS 18216+6418, reside in clusters. They present soft

Table 3. *Chandra* observations description.

Source	Instrument	Grating	Exp. time. [ks]	Obs. date
IRAS 09104+4109	ACIS-S	None	9.17	1999-11-03
IRAS 18216+6418	ACIS-S	LETG	171.82	2001-01-18

extended emission from the intra-cluster medium (ICM). To take into account this residual foreground in the subsequent spectral analysis, we added an XSPEC thermal component to the spectral model. Two parameters characterize this model: temperature and normalization.

We estimated the temperature of the cluster extracting an X-ray spectrum in an annular region around the source and fitted it with a thermal bremsstrahlung model. The normalization was obtained re-normalizing the flux from the annulus to that from the source circular region. To this end, we integrated the X-ray surface brightness profile of the cluster over both regions[1].

We determined the brightness profile using public *Chandra* data (see Table 3). Assuming an isothermal ICM, the radial profile of a cluster can be well-fit using a β-model (Sarazin 1986; Mushotzky 2004). This profile was then convolved with the XMM-*Newton* PSF, before integrating it over the regions of interest.

3.4. Spectral analysis

Our aim is to estimate the AGN and SB contribution to the total X-ray emission. The general model of the X-ray spectrum emitted by an AGN has typically four components: an underlying absorbed power law[2], a reflection component, an iron K_α emission line and a soft excess above the power law at energies below ~1 keV.

The typical power law photon index for AGN is $\Gamma \simeq 1.5-2.1$ (Nandra & Pounds 1994; Reeves & Turner 2000; Mateos et al. 2005). The soft excess component, common in type 1 AGN (Reeves & Turner 2000; Piconcelli et al. 2005), can be fitted with a thermal model, with an expected temperature remarkably constant around 0.1–0.3 keV (Piconcelli et al. 2005; Gierliński & Done 2006). The ratio between the luminosity of the soft excess component and the power law component in the soft band (0.5–2 keV) is ~0.15−1.45 (Piconcelli et al. 2005). The X-ray-to-bolometric luminosity ratio in the hard band (2–10 keV) for an AGN is ~0.015 (Elvis et al. 1994; Risaliti & Elvis 2004, see Sect. 4).

Several models have been proposed for the origin of the observed soft excess in AGN, such as a relativistically blurred photoionized disc reflection (Ross & Fabian 1993; Crummy et al. 2006) or ionized absorption in a wind from the inner disc (Gierliński & Done 2004, 2006). It has also been shown that the analysis of the high resolution XMM-*Newton* RGS spectra is important to understand the nature of the soft excess emission (Bianchi et al. 2006). We have only used thermal models in this paper for simplicity, since more detailed models are not warranted by the quality and low spectral resolution of the data. A deeper analysis of the soft excess emission of these sources will be presented elsewhere.

[1] The background spectrum of the annular region was extracted in a circular region free of sources away from the cluster emission. We used the XMM-*Newton* "blank fields" (Read & Ponman 2003) to extract the background spectrum of the source.

[2] $\frac{dN}{d\varepsilon dt} \propto \varepsilon^{-\Gamma}$, where N are the number of counts and ε is the energy of the counts.

The SB emission can be modeled with a power law with a typical photon index $\Gamma \simeq 1.0-1.4$ (White et al. 1983; Dahlem et al. 1998; Persic & Rephaeli 2002), or with a thermal model with temperature 0.5−1.0 keV (Iwasawa 1999; Franceschini et al. 2003). The soft X-ray-to-bolometric luminosity ratio for a SB is $\sim 10^{-4}$, as found by Iwasawa (1999) for a sample of four prototype powerful FIR SB galaxies. We can use this to estimate the bolometric luminosity of the sources.

All sources were analyzed using the following scheme. First we fitted the data with a power law model plus Galactic absorption[3] (see Table 4, Col. 3). We added intrinsic absorption (XSPEC `zpha` model) where it was statistically significant[4].

We compared this model with a power law reflected from neutral material (modeled with the XSPEC `pexrav`[5], Magdziarz & Zdziarski 1995). When two models had the same number of parameters (and hence the F-test is not useful), the fit with the lowest χ^2 was taken as our baseline model. However, when the χ^2 from two models were comparable, we adopted as our baseline fit that with less uncertainty in the determination of the model parameters.

We then checked for any significant additional component: iron emission line (modeled with `zgauss` at ~6.4 keV) and/or soft excess. We fitted the latter with different thermal models (blackbody: `zbbody`; bremsstrahlung: `zbremss`, Kellogg et al. 1975; bremsstrahlung with emission lines: `mekal`, Mewe et al. 1985; Kaastra & Mewe 1993). We introduced this thermal component to parameterize the starburst emission and/or the AGN soft excess emission.

In those cases where Γ was out of the range expected for AGN or SB, this parameter was fixed to 2, and we tried to fit again the spectrum with an absorbed power law and a reflection model (`pexrav`). In both cases, additional intrinsic absorption and thermal emission models were also added (if needed) to improve the fit.

The best fit model for each source is given in Table 4. We calculated the luminosity for each component in the hard and soft X-ray bands, corrected by Galactic and intrinsic absorption. A more detailed description of the analysis and the results for each source is presented in Sect. 3.5.

We estimated upper limits (see Table 4, Col. 11) for a thermal component in the X-ray spectra of those sources where it was not significant. To this end, we fixed all parameters to their best fit values. We added a thermal component (`zbremss`) with a fixed temperature, $kT = 0.6$ keV (the mean temperature of the ULIRGs thermal component from Franceschini et al. 2003), and we calculated the 2σ confidence interval for the normalization parameter, which was then used to estimate the upper limit of the luminosity.

3.5. Source by source analysis

IRAS 00182-7112

This type 2 QSO was detected only in the EPIC-PN camera. We modeled the spectrum of IRAS 00182-7112 with a reflection component, using the `pexrav` model

[3] All models referred to in this paper include a multiplicative Galactic absorption component fixed at the Galactic N_H value from Dickey & Lockman (1990).

[4] To this end we used the F-test, accepting additional spectral components only when they improved the fit with a significance $\geq 3\sigma$.

[5] We kept fixed all the parameters of the `pexrav` model to the standard values except the photon index of the incident power law, the reflection scaling factor and the normalization.

Table 4. XMM-*Newton* spectral analysis results. Fluxes and luminosities in CGS units. All errors are quoted at 90% confidence level for one parameter of interest (i.e. $\Delta\chi^2 = 2.71$) throughout this paper.

Source	Model [a]	$N_{\rm H}$ [b]	Γ	kT	EW	χ^2/ν	$\Delta\chi^2$	$\log S_{\rm X}$ [c]	$\log L$ [d]			
				(keV)	(keV)				$L_{\rm PL}^{\rm SX}$	$L_{\rm TH}^{\rm SX}$	$L_{\rm PL}^{\rm HX}$	$L_{\rm TH}^{\rm HX}$
IRAS 00182-7112	D + E	4.24	2, $E_c = 9^{+21}_{-4}$	–	0.8 ± 0.6	5.0/9	10.7	–12.8	44.9	<41.9	44.8	<40.7
IRAS F00235+1024	–	5.07	2	–	–	–	–	<–14.5	<42.2	–	<42.4	–
IRAS 07380-2342	–	64.3	2		–	–	–	<–13.7	<41.7	–	<42.5	–
IRAS 09104+4109	(B)[e] + A + E	1.82	1.62 ± 0.07	–	$0.38^{+0.10}_{-0.11}$	374/324	42	–11.7	44.2	<43.0	44.5	<41.8
+*Beppo*SAX:	(B)[e] + B + D + E	"	$1.2^{+0.3}_{-0.2}$	$3.1^{+0.4}_{-0.3}$	$0.2^{+3.4}_{-0.1}$	330/326	53	"	44.7	44.2	45.3	44.2
PG 1206+459	A	1.31	1.7 ± 0.9	–	–	72/67	–	–12.5	45.8	<44.0	45.1	<42.8
PG 1247+267	A + C	0.90	$1.98^{+0.05}_{-0.07}$	$0.49^{+0.23}_{-0.17}$	–	235/281	30	–12.3	45.9	45.5	45.9	44.0
IRAS F12509+3122	A + B	1.24	$1.38^{+0.11}_{-0.12}$	0.21 ± 0.03	–	38/30	80	–12.9	43.8	43.8	44.3	40.2
IRAS 12514+1027	B + F × A[f]	1.67	2	$0.35^{+0.17}_{-0.07}$	–	5/15	15	–14.2	43.2	42.2	43.3	39.7
IRAS 13279+3401	–	0.99	2	–	–	–	–	<–14.2	<42.1	–	<42.2	–
IRAS 14026+4341	–	1.19	2	–	–	–	–	<–13.7	<42.5	–	<42.6	–
IRAS F14218+3845	A	0.93	2.24 ± 0.12	–	–	70/75	–	-13.1	44.7	<43.8	44.6	<42.5
IRAS F15307+3252	A	2.03	2.1 ± 0.4	–	–	16/22	–	–13.6	45.4[g]	<43.1	45.5[g]	<41.9
IRAS 16347+7037	C + A	4.48	1.77 ± 0.13	1.53 ± 0.18	–	561/547	26	–11.7	45.8	45.7	46.0	45.4
IRAS 18216+6418	(C)[e] + C + A	4.04	$1.57^{+0.10}_{-0.12}$	$0.49^{+0.09}_{-0.08}$	–	329/332	151	–10.7	45.2	45.1	45.6	43.6

[a] XSPEC models: A: `power law`, B: `mekal`, C: `zbremss`, D: `pexrav`, E: `zgauss` (emission line), F: `zpha` (intrinsic absorption). [b] Galactic neutral hydrogen column density (in units of 10^{20} atoms cm^{-2}), from Dickey & Lockman (1990). [c] Observed frame 0.5–10 keV flux. [d] Rest frame intrinsic X-ray luminosity. SX: Soft X-ray (0.5–2 keV) band; HX: Hard X-ray (2–10 keV) band; PL: Power law component; TH: Thermal (soft excess) component. [e] This component models the cluster contribution. [f] Intrinsic $N_{\rm H} = 4^{+20}_{-3} \times 10^{23}$ cm^{-2}. [g] Luminosity corrected assuming Panessa et al. (2006) results. See Sect. 3.5 for details.

(Magdziarz & Zdziarski 1995). The photon index is fixed to 2 and a pure reflection component is assumed. This implies a lower limit to the column density of the absorber material ($N_{\rm H} > 10^{25}$ cm^{-2}). We marginally detect a narrow emission line at $6.75^{+0.08}_{-0.11}$ keV (significance $2-3\sigma$), consistent with He-like Fe line (this energy is also consistent at 2σ level with neutral Fe 6.4 keV line).

ISO and *Spitzer* IR data suggest the presence of a deeply obscured nuclear power source (Tran et al. 2001; Spoon et al. 2004). This is qualitatively consistent with our X-ray analysis results. The X-rays detected by XMM-*Newton* should be the reflected emission from the AGN, and the line is an iron K_α fluorescent emission from the reflecting material. The equivalent width of this line, 0.8 ± 0.6 keV, is consistent with the CT hypothesis, but the poor quality of the spectrum prevents us from reaching any stronger conclusion. Assuming that the direct X-ray emission is completely absorbed by CT material, we found that the intrinsic 2–10 keV luminosity of the AGN responsible for the reflection component is $6.3 \times 10^{44}(2\pi/\Omega_{\rm refl})$ erg s^{-1}, where $\Omega_{\rm refl} < 2\pi$ is the solid angle subtended by the reflector at the illuminating source. This X-ray emission gives an estimate to the bolometric luminosity of the AGN of $\sim 1.1 \times 10^{13}\ L_\odot$, which is consistent with the IR observations (see Figs. 2 and 3).

In conclusion, our X-ray analysis of this source points to an AGN with CT obscuration.

IRAS F00235+1024

XMM-*Newton* observed this NL SB galaxy for 26 ks, but it was not detected by the EPIC cameras. Wilman et al. (2003), assuming a thermal `mekal` model ($kT = 0.5$ keV), estimate an upper limit to the 0.5–2 keV luminosity of 2.8×10^{42} erg s^{-1}, consistent with our result in this band. The limit in the soft band implies a weak SB emission in X-rays, compared to that expected from the IR luminosity (Farrah et al. 2002a, see Table 5). Their upper limit to the hard X-ray luminosity ($\sim 1.9 \times 10^{44}$ erg s^{-1}) is also consistent with ours.

IRAS 07380-2342

This NL object has not been detected by XMM-*Newton*.

IRAS 09104+4109

The type 2 QSO IRAS 09104+4109 resides in a rich cluster (Kleinmann et al. 1988). The X-ray soft extended emission from the ICM was already detected by *ROSAT* (Fabian & Crawford 1995). We subtracted this foreground as explained in Sect. 3.3.

The source spectra were extracted from a circular region of 20″ for all detectors, and the cluster spectra from an annular region between 20″ and 90″ (constrained to the CCD where the source is located). The cluster emission was fitted with a `mekal` model. The temperature is $kT = 5.5 \pm 0.4$ keV, and the metal abundance is $0.30 \pm 0.12\ Z_\odot$, which is consistent with the mean Fe abundance for clusters with a temperature greater than 5 keV (Baumgartner et al. 2001). We obtained the radial brightness profile using *Chandra* data: a β-model with a core radius of $4\farcs6 \pm 0\farcs6$ and $\beta = 0\farcs576^{+0\farcs018}_{-0\farcs016}$.

The cluster emission represents 62% of the total 0.5–10 keV luminosity. The spectrum of the source was fitted with a power law with a Fe Kα broad ($\sigma = 0.27 \pm 0.09$ keV) emission line at $6.61^{+0.08}_{-0.10}$ keV. This broad line could be explained as a complex of neutral and ionized narrow lines merged due to the low resolution of the detector.

Although IRAS 09104+4109 is classified as a type 2 QSO, the XMM-*Newton* data did not reveal any intrinsic absorption feature. However, the *Chandra* observation of this source suggested a column density of 3×10^{23} cm^{-2} (Iwasawa et al. 2001). Also, *Beppo*SAX detected this object at energies greater than 10 keV, pointing to non-thermal quasar emission emerging from a thick absorbing torus (Franceschini et al. 2000), with $N_{\rm H} \sim 7 \times 10^{24}$ cm^{-2}.

Our combined analysis of the *Beppo*SAX and XMM-*Newton* data sets (which will be taken as the best fit for this source in what follows) shows that a reflection-only model is needed to explain the complete spectrum in the 0.2 to

50 keV range. This implies a lower limit ($N_{\rm H} > 10^{25}$ cm^{-2}) to the column density of the absorber, which it is consistent with Iwasawa et al. (2001), where a similar analysis of this source is done with *Beppo*SAX and *Chandra* observations. Assuming $\Gamma = 1.4$, which is in the flatter side of the photon index distribution of quasars (Reeves & Turner 2000), they found that a cold reflection model without transmitted component fits well the complete data.

This model gives an intrinsic hard X-ray luminosity of $2 \times 10^{45}(2\pi/\Omega_{\rm refl})$ erg s^{-1} for the AGN. The estimated bolometric luminosity of this source is then $\sim 3.5 \times 10^{13}\ L_{\odot}$, which is consistent with its IR data (see Figs. 2 and 3).

We have also found in our combined analysis a new thermal component, but its temperature ($kT \sim 3$ keV) is too high to be associated with SB or AGN emission. Since there is no evidence of a SB component in the IR SED of this source (Rowan-Robinson 2000), this thermal component is probably due to an incomplete subtraction of the cluster emission. Previous results indicate that a strong cooling flow of the ICM is taking place in the core of the cluster (Fabian & Crawford 1995; Allen & Fabian 1998; Ettori & Fabian 1999; Iwasawa et al. 2001), so the isothermal ICM hypothesis we have assumed could underestimate the cluster luminosity in the central region.

We confirm that IRAS 09104+4109 is probably a CT source, and that the X-ray emission detected below 10 keV by XMM-*Newton* is only a reflection continuum from cold matter.

PG 1206+459

The XMM-*Newton* observation of this QSO is contaminated by background flares at the beginning and at the end of the observation. The final effective exposure is ∼7 ks. The spectra continuum has been modeled with a power law. We have not detected significant intrinsic absorption or soft excess. The lack of absorption in the X-ray spectra is consistent with the optical and IR evidence (Haas et al. 1998; Rowan-Robinson 2000). Its hard X-ray luminosity is 1.3×10^{45} erg s^{-1}, which gives a bolometric luminosity of $\sim 2.2 \times 10^{13}\ L_{\odot}$, in agreement with the IR data (see Figs. 2 and 3). The X-ray spectrum of this object is therefore consistent with having a pure AGN origin.

PG 1247+267

The X-ray spectrum of this QSO has been modeled as a power law and a thermal component. A `pexrav` model is formally the best fit ($\chi^2/\nu = 224/282$) of these data. However, the photon index obtained ($\Gamma \sim 2.3$) with this model is slightly larger than that expected for an AGN. Moreover, the reflection scaling factor (∼4) is quite a lot larger than that typically expected for type 1 sources (within 0 and 1). No other reflection features have been found in the X-ray spectrum. Therefore, we have adopted the power law plus thermal component as our best fit. The bolometric luminosity of the AGN is $\sim 1.4 \times 10^{14}\ L_{\odot}$, using its hard X-ray luminosity. This result is consistent with the IR observations (see Figs. 2 and 3).

The temperature of the thermal component ($kT = 0.48^{+0.23}_{-0.17}$ keV) is consistent with the typical temperature of a SB galaxy. However, the bolometric luminosity that we can estimate through the soft X-ray emission for this SB is $\sim 10^{49}$ erg s^{-1}, much higher than the Rowan-Robinson (2000) estimate ($< 5.2 \times 10^{46}$ erg s^{-1}). Therefore, the soft excess component is too luminous to have a pure SB origin. Furthermore, its soft excess-to-power law soft X-ray luminosity ratio is ∼0.4, which is typical for soft excess observed in AGN. The X-ray spectrum of this source is consistent with being dominated by an AGN.

IRAS F12509+3122

A significant fraction (∼50%) of the observation time of this QSO is affected by high background. The PN and MOS spectra can be fitted by a power law model and a thermal component with $kT = 0.21 \pm 0.03$ keV, at a lower energy than that expected for a standard SB, but consistent with soft excess originating in an AGN. The bolometric luminosity inferred from the X-ray thermal luminosity is one order of magnitude greater than the estimate for a SB using IR data (Farrah et al. 2002a). The thermal-to-power law luminosity ratio is ∼1.2, in the range of AGN soft excess. The X-ray spectrum of this source is also AGN-dominated.

IRAS 12514+1027

This Seyfert 2 galaxy was also observed by *ROSAT* (Wilman et al. 1998), but only XMM-*Newton* has been able to detect its X-ray emission. Wilman et al. (2003) considered only the PN spectrum, modeled with a reflection component (`pexrav`, with fixed $\Gamma = 2$) and a thermal component (`mekal`, $kT = 0.31^{+0.13}_{-0.05}$ keV) corrected by intrinsic absorption ($N_{\rm H} = 1.3^{+0.9}_{-0.7} \times 10^{21}$ cm^{-2}). The resulting χ^2/ν is 8.5/12.

In our analysis, the three EPIC spectra were coadded (see Sect. 3.1). We modeled the spectrum with an absorbed power law with a photon index fixed to 2, and a thermal component.

The temperature of the thermal component is $kT = 0.35^{+0.17}_{-0.07}$ keV, consistent with that usually observed in a SB galaxy. The soft component-to-power law luminosity ratio is slightly lower than that associated with an AGN. The 0.5–2.0 keV luminosity of this soft component is 1.5×10^{42} erg s^{-1}, which implies a bolometric luminosity for the SB of $\sim 1.5 \times 10^{46}$ erg s^{-1}. The IR luminosity of the SB estimated from the analysis of the IR SED of the source is $\sim 5 \times 10^{46}$ erg s^{-1} (Rowan-Robinson 2000). This thermal component could be consistent with a SB origin.

The optical, IR and X-ray data point to a CT quasar and a SB of comparable bolometric luminosities.

IRAS 13279+3401

This QSO has not been detected by XMM-*Newton*.

IRAS 14026+4341

The XMM-*Newton* observation of this QSO 1.5 is heavily contaminated by background flares. All the PN data are affected by count rate background greater than 15 counts per second. The MOS data have a brief interval free of flares, but the source is not detected.

IRAS F14218+3845

The QSO IRAS F14218+3845 was observed by XMM-*Newton* in two occasions. The second observation was heavily affected by high radiation background. We co-added the six spectra of the different observations to increase the S/N ratio. The spectrum was modeled with a power law. No significant soft excess or intrinsic absorption was found.

Table 5. Flux and luminosity data of the sample.

		Flux density (Jy)[a]				IR	log L (erg s^{-1})				
Source	R[b]	12 μm	25 μm	60 μm	100 μm	Model[c]	$L_{\rm FIR}$[d]	$L_{\rm IR}$[d]	$L_{\rm IR,RR}$	$L^{\rm AGN}_{\rm IR,RR}$	$L^{\rm SB}_{\rm IR,RR}$
IRAS 00182-7112	17.738	<0.06025	0.133 ± 0.010	1.20 ± 0.08	1.19 ± 0.12	S+A	46.49	<46.72	<46.93	<46.48	46.74
IRAS F00235+1024	>21.5	<0.173	<0.193	0.43 ± 0.06	<0.94	S+A	<46.76	<47.27	46.74	46.44	46.45
IRAS 07380-2342	16.869	0.48 ± 0.03	0.80 ± 0.08	1.17 ± 0.09	3.5 ± 0.3	A+S	46.56	47.08	46.97	46.79	46.48
IRAS 09104+4109	17.819	0.13 ± 0.03	0.334 ± 0.013	0.53 ± 0.04	<0.44	A	<46.42	<46.99	<46.92	46.84	<46.15
PG 1206+459 [d]	15.135	0.21 ± 0.04	<0.113	0.26 ± 0.05	0.35 ± 0.07	A	47.20	<47.94	<47.80	47.78	<46.57
PG 1247+267 [d]	14.621	<0.126	<0.113	0.24 ± 0.05	0.17 ± 0.03	A	47.70	<48.39	<47.94	47.91	<46.76
IRAS F12509+3122	16.590	<0.106	0.10 ± 0.03	0.22 ± 0.04	<0.675	A+S	<46.86	<47.37	47.00	46.76	46.62
IRAS 12514+1027	17.654	<0.0632	0.190 ± 0.016	0.71 ± 0.06	0.76 ± 0.15	S+A	46.18	<46.51	46.63	46.27	46.39
IRAS 13279+3401	15.689	<0.0937	<0.126	1.18 ± 0.08	1.20 ± 0.18	A+S	46.58	<46.84	46.53	46.36	46.04
IRAS 14026+4341	15.651	0.12 ± 0.03	0.285 ± 0.014	0.62 ± 0.06	0.99 ± 0.24	A+S	46.26	46.70	46.54	46.34	46.11
IRAS F14218+3845	>21.5	<0.0969	<0.075	0.57 ± 0.06	2.10 ± 0.17	S+A	47.80	<48.06	46.86	46.15	46.76
IRAS F15307+3252	19.131	<0.065	0.071 ± 0.019	0.23 ± 0.04	<0.71	A+S	<47.07	<47.46	47.22	47.05	46.73
IRAS 16347+7037 [e]	13.979	0.059 ± 0.010	0.122 ± 0.004	0.27 ± 0.05	0.35 ± 0.07	A+S	47.42	47.86	47.81	47.73	47.04
IRAS 18216+6418	13.403	<0.238	0.445 ± 0.012	1.24 ± 0.05	2.13 ± 0.17	A+S	46.49	<46.89	46.78	46.54	46.37

[a] Observed by *IRAS* (from NED). [b] UK-R magnitude (SuperCOSMOS Sky Survey). [c] AGN (A) and/or starburst (S) components needed to fit the IR SED (as in Table 1, Col. 3). First letter indicates the dominant component. [d] Infrared luminosities in the 40−500 μm (FIR) and 1−1000 μm (IR) bands, computed using *IRAS* fluxes (Sanders & Mirabel 1996). [e] 60 and 100 μm fluxes are *ISO* data from Haas et al. (2000).

The IR data suggest that this HLIRG is a SB dominated source (Verma et al. 2002; Farrah et al. 2002a), but our analysis of its XMM-*Newton* X-ray spectrum does not reveal any SB features. Using the upper limit that we have estimated (see Table 4) for a thermal component, the total SB luminosity is less than 6×10^{47} erg s^{-1}, which is consistent with the SB luminosity estimated by Farrah et al. (2002a) through IR and sub-mm data (6×10^{46} erg s^{-1}). Although a SB component cannot be excluded, the data point to an AGN-dominated X-ray emission (Franceschini et al. 2003).

IRAS F15307+3252

Previous observations with *ROSAT* and *ASCA* detected no X-ray emission from this QSO 2 (Fabian et al. 1996; Ogasaka et al. 1997). We detected a faint X-ray emission in the XMM-*Newton* public data. The observation of this source is affected by high background flares. The three EPIC extracted spectra were coadded to increase the S/N ratio. We fitted this spectrum using a power law. We were not able to find any absorption feature or thermal emission.

XMM-*Newton* has observed IRAS F15307+3252 on two more occasions, but the data are still private. Iwasawa et al. (2005), using the complete data set, found a prominent Fe Kα line at ∼6.5 keV, indicating the presence of a CT AGN. This is in agreement with optical spectropolarimetry data indicating the presence of a dust-enshrouded quasar (Hines et al. 1995). The estimate of the AGN bolometric luminosity using the observed emission line luminosity is also consistent with previous results (Yun & Scoville 1998; Aussel et al. 1998; Verma et al. 2002; Peeters et al. 2004). The hard X-ray emission detected by us is probably reflected radiation, because of CT obscuration. Panessa et al. (2006) found that the ratio between the intrinsic and the observed X-ray luminosity in CT Seyfert galaxies is ∼60. We have corrected the X-ray luminosity calculated with the public XMM-*Newton* data by this factor. The resulting hard X-ray luminosity (∼3.2×10^{45} erg s^{-1}) is consistent with the estimate given by Iwasawa et al. (2005) ($L_{\rm X} > 1 \times 10^{45}$ erg s^{-1}), using the luminosity of the iron emission line. Assuming an AGN origin, this X-ray emission gives a bolometric luminosity for this source of ∼5.5×10^{13} $L_\odot$, in agreement with the IR data (see Figs. 2 and 3).

Iwasawa et al. (2005) also found extended soft emission, with $kT = 2.1^{+0.6}_{-0.4}$ keV. They identify this extended emission with hot gas associated with a relatively poor cluster around this object. Although no galaxy cluster has been found associated with this source, an *HST* observation shows a moderate galaxy overdensity. Moreover, its bolometric luminosity to temperature relation would be similar to that typical of poor clusters (Fukazawa et al. 2004).

In summary, the X-ray spectrum of this source is consistent with the emission originating in a CT AGN.

IRAS 16347+7037

The spectrum of the QSO IRAS 16347+7037 was modeled with a power law and a thermal component. No intrinsic absorption is detected.

The XMM-*Newton* X-ray spectrum is consistent with a type 1 AGN spectrum, as the optical (Evans et al. 1998) and IR (Haas et al. 1998; Farrah et al. 2002b) observations suggest. Previous X-ray data from *ASCA* were also consistent, and there was no evidence of iron Kα emission feature or any absorption edge (Nandra et al. 1995).

The soft excess has $L(0.5{-}2.0\,{\rm keV}) = 5.6{\times}10^{45}$ erg s^{-1}. This would imply a SB bolometric luminosity three orders of magnitude greater than the SB luminosity calculated with the IR data (Farrah et al. 2002b, see Table 5). Therefore this component is unlikely to be associated with a SB. Moreover, its thermal-to-power law luminosity ratio is consistent with a soft excess from the AGN.

This model gives a bolometric luminosity for the AGN of ∼2.2×10^{14} $L_\odot$, in agreement with the IR observations of this source (see Figs. 2 and 3). Our analysis points to a pure AGN origin for the X-ray spectrum, in agreement with the optical and IR data.

IRAS 18216+6418

The PN data of this QSO 1.2 were heavily affected by pile-up, so we used only the MOS data. The source spectra were extracted from a 20″ radius circular region in both MOS detectors. This QSO is located in a rich cluster, and *ROSAT* detected the

ICM thermal emission (Saxton et al. 1997; Hall et al. 1997). We subtracted the soft X-ray emission from the cluster, as explained in Sect. 3.3.

The MOS cameras operated in small-window mode, so we considered the PN image to model the cluster (the pile-up only affects the central region of the source). We extracted a spectrum from an annular region between 20″ and 80″ (constrained to the CCD where the source is located). The resulting temperature of the `zbremss` model was $kT = 2.3^{+1.0}_{-0.6}$ keV. We also used the radial X-ray brightness profile published by Fang et al. (2002), (core radius of $17''.6 \pm 0''.17$, $\beta = 0''.74^{+0''.05}_{-0''.03}$), to renormalize the cluster model. The cluster X-ray emission is 32% of the total 0.5–10 keV luminosity.

The source spectrum best fit is a power law ($\Gamma = 1.57^{+0.10}_{-0.11}$) with a soft thermal component. A `pexrav` model is formally the best fit ($\chi^2/\nu = 321/333$) of this spectrum. As discussed in PG 1247+267, the steeper photon index ($\Gamma \sim 2.3$) and the reflection scaling factor $\gg 1$ ($R \sim 15$) led us to adopt the power law plus thermal component as our best fit.

The photon index of the power law is not consistent with previous X-ray observations with *ASCA* ($\Gamma = 1.75 \pm 0.03$, Yamashita et al. 1997) and *Chandra* ($\Gamma = 1.761^{+0.047}_{-0.052}$, Fang et al. 2002).

In Fig. 1j a systematic effect in the $\Delta\chi^2$ spectrum can be seen above 5 keV. This may be due to a bad extraction of the cluster emission or to the use of the blank-field background. If we ignore the data above 4.5 keV, we get a steeper photon index ($\Gamma = 1.68 \pm 0.11$), compatible with previous X-ray observations.

A thermal component is also detected, with a temperature of $0.49^{+0.09}_{-0.08}$ keV, consistent with SB emission. However, if this emission were associated with the SB, the bolometric luminosity of the SB would be three orders of magnitude higher than the luminosity calculated using the IR data (Farrah et al. 2002a). The soft component-to-power law luminosity ratio is in the range of that typically observed in an AGN.

Ginga (Kii et al. 1991), *ASCA* (Yamashita et al. 1997) and *Chandra* (Fang et al. 2002; Yaqoob & Serlemitsos 2005) detected iron emission features in this HLIRG. Jiménez-Bailón et al. (2007) detected a Fe-K emission line with a complex structure in the PN XMM-Newton spectrum of this source. We also detected an emission line in the 6–7 keV rest frame band, but the significance of the detection ($<2\sigma$) was below our adopted threshold, and therefore we have not considered it further. We estimated a 3σ flux upper limit to a broad ($\sigma = 0.1$ keV) line component at 6.4 keV of $<3 \times 10^{-5}$ photons cm^{-2} s^{-1}, consistent with the value $\sim(3 \pm 1) \times 10^{-5}$ photons cm^{-2} s^{-1} obtained with the *Chandra* data (Fang et al. 2002).

Assuming an AGN origin, the hard X-ray emission gives a bolometric luminosity for this source of $\sim 7 \times 10^{13}\ L_\odot$, in agreement with its IR data (see Figs. 2 and 3). The X-ray spectrum of this object is consistent with a pure AGN origin.

4. Discussion

In their study of X-ray emission from ULIRGs, Franceschini et al. (2003) define that the X-ray emission of a ULIRG is AGN-dominated if it presents either: a) a high X-ray luminosity, $L(2-10\ \mathrm{keV}) > 10^{42}$ erg s^{-1}; b) a heavily obscured hard X-ray component with $N_\mathrm{H} > 10^{22}$ cm^{-2} (very flat or inverted hard X-ray spectra); or c) a Fe-K emission complex at ~6.4 keV with equivalent width $\gtrsim 1$ keV (iron fluorescent emission from material illuminated by the AGN). The ten detected HLIRGs from our sample present at least one of the three characteristics above, thus showing an AGN-dominated X-ray spectrum.

This result is in agreement with the trend noted by Veilleux et al. (1999) for ULIRGs: the fraction of sources with Seyfert characteristics increase with L_IR (from ~25% among ULIRGs with $L_\mathrm{IR} < 10^{12.3}\ L_\odot$ to ~50% among those with $L_\mathrm{IR} > 10^{12.3}\ L_\odot$). However, we must keep in mind that our sample is not complete, and could be slightly biased towards AGN. The first subsample in Rowan-Robinson (2000), which is not biased in favor of AGN (see Sect. 2), presents 50% of objects with Seyfert characteristics.

Five objects from our sample (four type 2 objects and one NL object) are probably CT, as reported in the literature. Our analysis of the XMM-*Newton* data of two sources (IRAS 00182-7112, IRAS 12514+1027) are consistent with the CT hypothesis, as well as our combined analysis of XMM-*Newton* and *Beppo*SAX data for IRAS 09104+4109. IRAS F00235+1024 has not been detected, probably because it is heavily obscured. We have found no absorption features in IRAS F15307+3252, but as explained in Sect. 3.5, recently published results from XMM-*Newton* private data are consistent with CT absorption (Iwasawa et al. 2005).

We calculated the FIR (40–500 μm) luminosities (L_FIR) using the *IRAS* fluxes (Sanders & Mirabel 1996, see Table 5, Col. 7). In Fig. 2 we plotted the 2–10 keV luminosity of the power law component for each source versus the FIR luminosity. We included the ULIRGs data from Franceschini et al. (2003) and the high-z QSO from Stevens et al. (2005) for comparison. No correlation between the 2–10 keV and the FIR luminosity is found in HLIRGs, although it must be kept in mind that the sample is not complete in any sense.

We estimated the expected X-ray luminosity for a standard AGN, given its FIR luminosity. To this end, we calculated the 2–10 keV-to-FIR luminosity ratio typical of nearby bright QSOs, using their mean SED. Since the original Elvis et al. (1994) sample was biased towards sources with high X-ray luminosity, we employed the Risaliti & Elvis (2004) new data on QSO SED. Using this corrected SED, the ratio of the 2–10 keV band to bolometric luminosity changes significantly by a factor of 2, from ~0.03 to ~0.015. The X-ray luminosity derived from the IR luminosity using the latter ratio is plotted in Fig. 2 with a thick solid line. The top area between thin lines ("AGN-zone") is the dispersion of the SED, calculated with the 90 percentile distribution (Elvis et al. 1994).

We can also calculate a relationship between FIR and X-ray luminosity for SB galaxies. The SFR of a SB is given by its FIR luminosity by $SFR_\mathrm{FIR} \sim L_\mathrm{FIR}/2.2 \times 10^{43}\ M_\odot\ \mathrm{yr}^{-1}$ (Kennicutt 1998), and by its 2–10 keV X-ray luminosity by $SFR_\mathrm{X} \sim L_{2-10}/10^{39}\ M_\odot\ \mathrm{yr}^{-1}$ (Persic et al. 2004, all luminosities are in CGS units). Assuming equal SFR, the 2–10 keV to FIR luminosity ratio is $L(2\text{–}10\ \mathrm{keV})/L_\mathrm{FIR} \sim 4.5 \times 10^{-5}$. This relation is shown in Fig. 2 as the lower thick solid line ("SB-line").

Most HLIRGs and all high-z QSO are in the "AGN-zone", while only the AGN-dominated ULIRGs and two HLIRGs seem to be composite sources: their X-ray luminosity is too high to be produced only by a SB (above the "SB-line"), and their FIR luminosity is too high to be produced only by an AGN (to the right of the "AGN-zone"). The SB-dominated ULIRGs are concentrated near the "SB-line". The upper limits for the X-ray-undetected HLIRGs seem to indicate that their hard X-ray emission comes only from SB activity. However, the X-ray emission of the non-detected sources could be affected by heavy obscuration. In fact, one of the non-detected sources, IRAS F00235+1024, is probably CT as seen from their IR spectrum so its X-ray emission could be depressed by heavy absorption. However the remaining sources are optical QSOs,

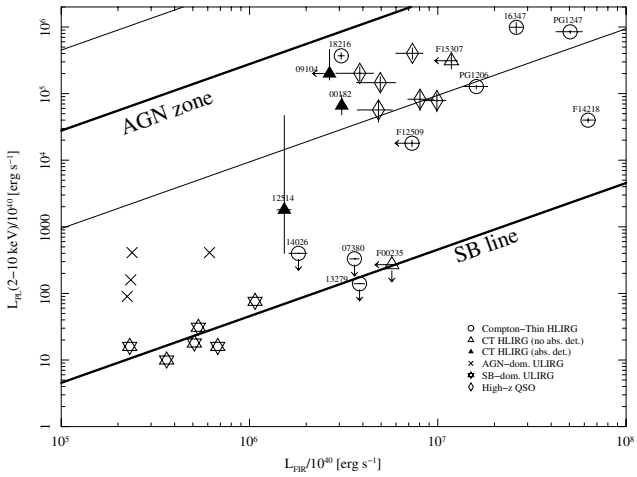

Fig. 2. 2–10 keV X-ray luminosity of the power law component versus FIR luminosity (40–500 μm). Filled symbols represent sources where we have detected X-ray absorption (models D or F in Table 4). The top thick solid line and area between the thin solid lines ("AGN-zone") indicate the X-ray luminosity expected for an AGN of a given FIR luminosity (90% dispersion, Elvis et al. 1994; Risaliti & Elvis 2004). The bottom thick solid line ("SB-line") indicates the X-ray luminosity expected for a SB of a given FIR luminosity (Persic et al. 2004; Kennicutt 1998). See Sect. 4 for details.

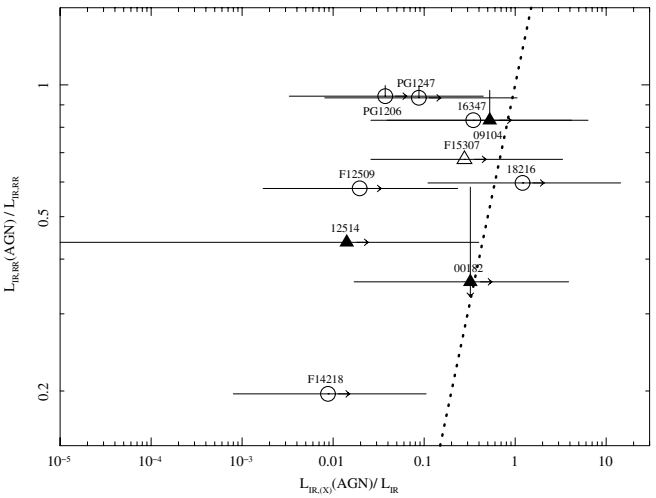

Fig. 3. AGN to total-IR luminosity ratio, calculated by Rowan-Robinson (2000), versus AGN (estimated through our X-ray data) to total (computed with the *IRAS* fluxes) IR luminosity ratio. The dotted line means equal values for the ratios. In the case of upper limits we plot as error bars the dispersion of X-ray-to-IR luminosity ratio from Elvis et al. (1994). IRAS F00235+1024, IRAS 07380-2342, IRAS F12509+3122, IRAS 12514+1027, IRAS 13279+3401, IRAS 14026+4341 and IRAS F14218+33845 IR data are taken from the Farrah et al. (2002a) results; IRAS F15307+3252 IR data is taken from the Verma et al. (2002) results; IRAS 16347+7037 IR data is taken from the Farrah et al. (2002b) results. Symbols as in Fig. 2.

where little or no absorption is expected. For example, the QSOs from Stevens et al. (2005) show relatively low absorption ($21 < \log N_{\rm H} < 22$ cm^{-2}). Recent XMM-*Newton* observations of these high-z HLIRGs suggest highly ionized winds with $22.5 < \log N_{\rm H} < 23.5$ cm^{-2} (Page et al. 2007). Further sensitive data on isotropic indicators (such as FIR or MIR or >10 keV emission) are needed to investigate the seemingly contradictory nature of these HLIRGs.

Note that if the Elvis et al. (1994) X-ray-to-FIR ratio is used instead of the Risaliti & Elvis (2004) ratio, only three HLIRGs (IRAS 09104+4109, IRAS 16347+7037 and IRAS 18216+6418) would lie on the "AGN-zone", and the rest would be considered as composite AGN/SB sources. This confirms the relevance of the Risaliti & Elvis (2004) correction.

The HLIRGs FIR emission is systematically above the Risaliti & Elvis (2004) estimate for a standard local QSO of the same X-ray luminosity (i.e., the sources are located on the right of the thick upper line in Fig. 2). This FIR excess could be associated with the SB activity in HLIRGs. Alternatively, this could also hint at a possible difference between the standard QSO SED and the AGN component of the HLIRGs SED. In this line, it has been shown that the shape of the SED is probably related to the luminosity (Marconi et al. 2004).

We attempted to unravel the origin of the excess infrared emission with respect to that predicted using the Risaliti & Elvis (2004) QSO SED. We estimated the AGN contribution to the total IR luminosity of the HLIRGs in two independent ways, in order to know if this IR excess comes from SB activity, or from an intrinsic difference in the AGN SED.

On one hand, Rowan-Robinson (2000) has modeled the IR SED of all sources in this sample with radiative transfer models, and estimated the contribution of the AGN dust torus ($L^{\rm AGN}_{\rm IR,RR}$) and the SB to the total IR luminosity (1–1000 μm, $L_{\rm IR,RR}$) (Table 5, Cols. 9 and 10 respectively). We have corrected the relative contribution of IRAS F00235+1024, IRAS 07380-2342, IRAS F12509+3122, IRAS 12514+1027, IRAS 13279+3401, IRAS 14026+4341, IRAS F14218+3845, IRAS F15307+3252 and IRAS 16347+7037 with the results of Verma et al. (2002), Farrah et al. (2002a) and Farrah et al. (2002b), where new IR and sub-mm data are used.

On the other hand, we calculated this ratio using the power law X-ray luminosity. We assume that this emission is associated with an AGN with a standard SED (Risaliti & Elvis 2004), and we calculate the IR-to-2–10 keV luminosity ratio, similarly to that calculated in Fig. 2. We obtain an independent estimate of the expected IR luminosity of the AGN ($L^{\rm AGN}_{\rm IR,(X)}$).

In Fig. 3 we compare the relative contribution of the AGN to the total IR luminosity calculated by Rowan-Robinson (2000), to our estimate obtained from X-ray data (we included only the X-ray detected sources). The dotted line corresponds to the 1:1 relation, i.e. an agreement between the two estimates. Most of the sources have lower limits on the abscissae because their 12 and 25 μm *IRAS* fluxes are upper limits (see Table 5).

Our estimates of the AGN relative contribution for all sources are formally consistent with those of Rowan-Robinson (2000). However, there seems to systematically be an overestimate of the IR AGN component from Rowan-Robinson (2000) with respect to the X-ray measurements.

The values of $L^{\rm AGN}_{\rm IR,(X)}/L_{\rm IR}$ plotted in Fig. 3 are independent of the SB luminosity, so this disagreement is probably due to the IR-to-X-ray ratio used to estimate the IR luminosity from the X-ray luminosity. This favors the hypothesis of an intrinsic difference between the standard QSO SED and the AGN component of the HLIRGs SED. A detailed radio-to-X-ray study of the spectral energy distribution of HLIRGs is needed to solve this question.

Figure 4 is a luminosity-luminosity plot of the soft X-ray excess versus power law components. In IRAS 09104+4109, IRAS F12509+3122, PG 1247+267, IRAS 16347+7037 and IRAS 18216+6418 the soft excess component is too luminous to come only from a SB (see Sect. 3.5 for a detailed description

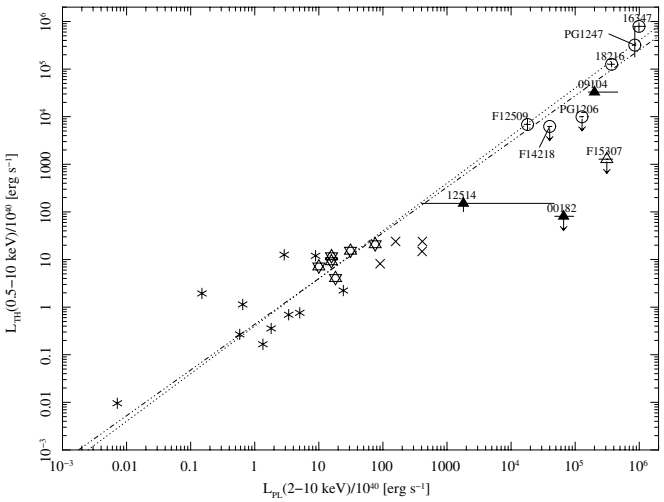

Fig. 4. L_X (0.5–10 keV) of the soft excess component versus L_X (2–10 keV) of the power law component. Asterisks represent SB galaxies from Franceschini et al. (2003). The dotted line is a correlation obtained by Franceschini et al. (2003) for SB-dominated ULIRGs. The dash-dotted line is a correlation for the SB-dominated ULIRGs and the SB galaxies samples calculated by us. The soft excess in IRAS 09104+4109 is probably associated with cluster emission (see Sect. 3.5 for details). Symbols as in Fig. 2.

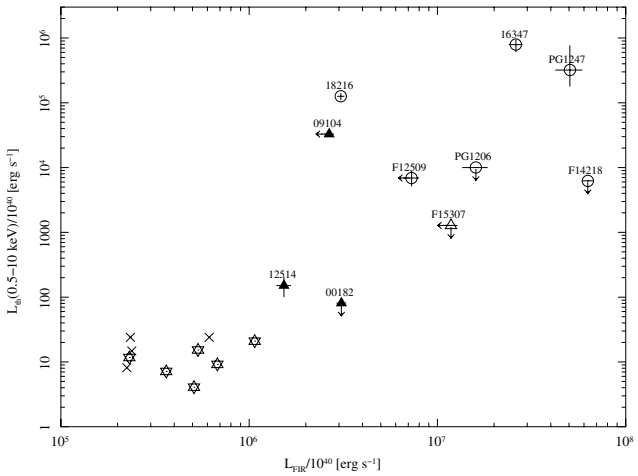

Fig. 5. L_X (0.5–10 keV) of the soft excess component versus FIR luminosity. The soft excess in IRAS 09104+4109 is probably associated with cluster emission (see Sect. 3.5 for details). Symbols as in Fig. 2.

of each source). In the case of IRAS 09104+4109 the soft excess is probably due to an incomplete subtraction of the cluster emission, while in the remaining four sources is probably of the same origin as in luminous QSO (Piconcelli et al. 2005).

An X-ray thermal component associated with SB emission has been observed in all ULIRGs from Franceschini et al. (2003). However, only in 1 out of 14 HLIRGs have we found a soft X-ray emission whose origin could be associated with SB activity.

Oddly, the above HLIRGs with AGN-like soft excess emission follow the correlation found for SB-dominated ULIRGs by Franceschini et al. (2003) (dotted line in Fig. 4). To increase the statistics and to test if this correlation holds at lower IR luminosities, we included a sample of SB galaxies (Franceschini et al. 2003, and references therein). We calculated a non-parametric correlation coefficient (generalized Kendall's Tau[6]) for the SB galaxies and the SB-dominated ULIRGs, finding $Z_\tau = 3.69$ with a significance level[7] of 99.98% ($>3\sigma$). The correlation slope is consistent with that obtained by Franceschini et al. (2003) for SB-dominated ULIRGs only.

We investigated the relationship between the X-ray soft excess component luminosity and the FIR luminosity (Fig. 5), finding no clear correlation. A test using generalized Kendall's Tau confirms this impression: $Z_\tau = 2.13$, with a significance level 96.66% ($<3\sigma$).

We also tested a possible cosmological evolution in the sample. We estimated the SFR for each source using its IR luminosity (Kennicutt 1998). Their SFR and 2–10 keV-to-IR-luminosity ratio versus redshift are plotted in Fig. 6. Cosmic star formation shows a large decline between $z \sim 2$ and the present day (Franceschini et al. 1999), so we expect an increment of the SFR of HLIRGs up to $z \sim 2$. Higher SFR at higher redshift is observed in the upper panel of Fig. 6. However the sources follow the lower envelope, which is the *IRAS* FSC sensitivity limit (solid line in Fig. 6), clearly indicating a selection effect. Therefore, we cannot draw conclusions about the dependence of SFR with redshift.

As shown in the bottom panel of the Fig. 6, the ratio of hard X-ray-to-FIR luminosity remains constant with z. This holds even if we subtract the FIR luminosity emitted by the AGN, calculated using the X-ray PL luminosity as in Fig. 3.

We have seen that the IR emission is consistent with an AGN origin, but if we assume that the IR excess shown in Fig. 2 is associated with the SB activity, Fig. 6 shows that its evolution must be similar to that of the X-ray emission. This, in turn, suggests that the presence of a SB and the occurrence of AGN activity through accretion onto a super-massive black hole are physically related. This result is in agreement with the coeval black hole/stellar bulge formation hypothesis (Granato et al. 2004; Stevens et al. 2005; Di Matteo et al. 2005).

5. Conclusions

We have performed a systematic X-ray study of a sample of 14 HLIRGs using XMM-*Newton* data from the archive, and our own private data. We modeled the X-ray spectra of each source, finding very heterogeneous spectral properties. Our results are summarized as follows:

1. All X-ray detected HLIRGs of the sample (ten sources) have AGN-dominated X-ray spectra.
2. No correlation is found between the 2–10 keV and IR luminosities in HLIRGs. The hard X-ray luminosity of most (eight) HLIRGs is consistent with emission from an AGN component only. However two HLIRGs (as well as all the AGN-dominated ULIRGs) seem to show a composite AGN/SB nature: their X-ray luminosity is too high to be produced only by a SB, and their IR luminosity is too high to be produced by only an AGN. The remaining four HLIRGs are undetected in X-rays.
3. The hard X-ray luminosity associated with the AGN is systematically below that expected for a local QSO (Elvis et al. 1994; Risaliti & Elvis 2004) of the same IR luminosity. This seems to suggest that there is an intrinsic difference between the AGN component of the HLIRGs SED and the SED of

[6] We employed the ASURV software for this test (Isobe et al. 1985, 1986).

[7] Note that even excluding the isolated source in the bottom left corner, this correlation remains almost unchanged.

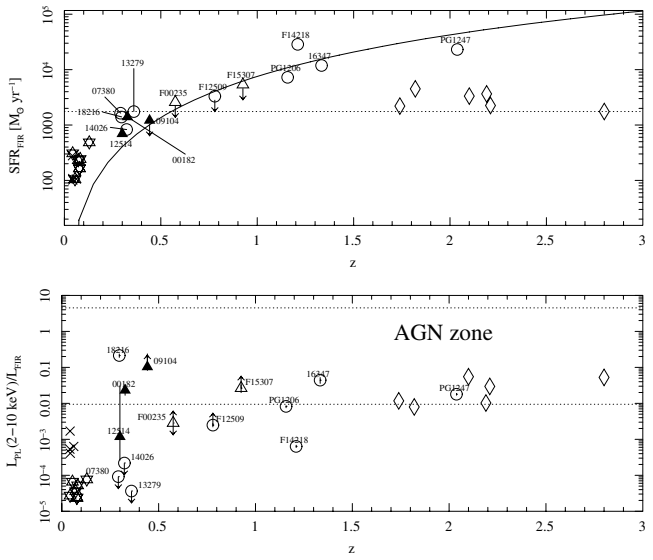

Fig. 6. Symbols as in Fig. 2. *Top*: SFR derived from FIR luminosity (Kennicutt 1998), versus redshift. The dotted line represents the SFR limit corresponding to the HLIRGs definition. The solid line is the SFR for a source with *IRAS* fluxes equals to the *IRAS* FSC sensitivity limits (Moshir et al. 1990). *Bottom*: 2–10 keV power law-X-ray-to-FIR luminosities ratio versus redshift. The area between the dotted lines represent the expected ratio for a quasar (with 90% of dispersion) with a standard SED (Elvis et al. 1994; Risaliti & Elvis 2004).

local QSOs. A detailed radio-to-X-ray study of the HLIRGs SED is needed to understand this issue.

4. There are five Compton-thick candidate sources in our sample, including all the type 2 AGN (four) and one starburst object undetected in X-rays. We found evidence for X-ray absorption in three of the type 2 AGN. Our analysis supports the Compton-thick nature of these sources.
5. We detected five HLIRGs with soft excess emission. Four sources present luminosities consistent with type 1 AGN soft excess. While all ULIRGs from Franceschini et al. (2003) present a soft X-ray thermal component associated with a SB, only in one HLIRGs did we find a soft excess probably associated with SB emission.
6. The hard-X-ray-to-FIR luminosity ratio remains constant with z, suggesting that the AGN and SB phenomena are physically connected in HLIRGs.

Acknowledgements. A.R. acknowledges support from a Universidad de Cantabria fellowship. F.P. acknowledges support by a "Juan de la Cierva" fellowship. Financial support for A.R., F.P. and F.J.C. was provided by the Spanish Ministry of Education and Science, under project ESP2003-00812.
This paper is based on observations obtained with XMM-*Newton*, an ESA science mission with instruments and contributions directly funded by ESA Member States and NASA; *Chandra*, a NASA mission; *Beppo*SAX, a project of the ASI (Italy) with participation of the NIVR (Netherlands) and the Space Science Department of ESA; *ISO*, an ESA project with the participation of ISAS and NASA; and *IRAS*, a joint project of the US, UK and the Netherlands. This research also has made use of the SuperCOSMOS Sky Survey (SSS) database and the NASA/IPAC Extragalactic Database (NED) which is operated by the Jet Propulsion Laboratory, California Institute of Technology, under contract with the National Aeronautics and Space Administration.

References

Allen, S. W., & Fabian, A. C. 1998, MNRAS, 297, L57
Armus, L., Heckman, T. M., & Miley, G. K. 1989, ApJ, 347, 727
Aussel, H., Gerin, M., Boulanger, F., et al. 1998, A&A, 334, L73
Baumgartner, W., Horner, D., & Mushotzky, R. 2001, BAAS, 33, 1337
Bianchi, S., Guainazzi, M., & Chiaberge, M. 2006, A&A, 448, 499
Crummy, J., Fabian, A. C., Gallo, L., & Ross, R. R. 2006, MNRAS, 365, 1067
Dahlem, M., Weaver, K. A., & Heckman, T. M. 1998, ApJS, 118, 401
Di Matteo, T., Springel, V., & Hernquist, L. 2005, Nature, 433, 604
Dickey, J. M., & Lockman, F. J. 1990, ARA&A, 28, 215
Ehle, M., Breitfellner, M., González Riestra, R., et al. 2005, XMM-Newton Users' Handbook, 2nd edn., XMM-Newton SOC Team
Elvis, M., Wilkes, B. J., McDowell, J. C., et al. 1994, ApJS, 95, 1
Ettori, S., & Fabian, A. C. 1999, MNRAS, 305, 834
Evans, A. S., Sanders, D. B., Cutri, R. M., et al. 1998, ApJ, 506, 205
Fabian, A. C., & Crawford, C. S. 1995, MNRAS, 274, L63
Fabian, A. C., Cutri, R. M., Smith, H. E., Crawford, C. S., & Brandt, W. N. 1996, MNRAS, 283, L95
Fang, T., Davis, D. S., Lee, J. C., et al. 2002, ApJ, 565, 86
Farrah, D., Serjeant, S., Efstathiou, A., Rowan-Robinson, M., & Verma, A. 2002a, MNRAS, 335, 1163
Farrah, D., Verma, A., Oliver, S., Rowan-Robinson, M., & McMahon, R. 2002b, MNRAS, 329, 605
Franceschini, A., Mazzei, P., de Zotti, G., & Danese, L. 1994, ApJ, 427, 140
Franceschini, A., Hasinger, G., Miyaji, T., & Malquori, D. 1999, MNRAS, 310, L5
Franceschini, A., Bassani, L., Cappi, M., et al. 2000, A&A, 353, 910
Franceschini, A., Aussel, H., Cesarsky, C. J., Elbaz, D., & Fadda, D. 2001, A&A, 378, 1
Franceschini, A., Braito, V., Persic, M., et al. 2003, MNRAS, 343, 1181
Fukazawa, Y., Makishima, K., & Ohashi, T. 2004, PASJ, 56, 965
Genzel, R., & Cesarsky, C. J. 2000, ARA&A, 38, 761
Gierliński, M., & Done, C. 2004, MNRAS, 349, L7
Gierliński, M., & Done, C. 2006, MNRAS, 371, L16
Granato, G. L., De Zotti, G., Silva, L., Bressan, A., & Danese, L. 2004, ApJ, 600, 580
Haas, M., Chini, R., Meisenheimer, K., et al. 1998, ApJ, 503, L109
Haas, M., Müller, S. A. H., Chini, R., et al. 2000, A&A, 354, 453
Hall, P. B., Ellingson, E., & Green, R. F. 1997, AJ, 113, 1179
Hines, D. C., Schmidt, G. D., Smith, P. S., Cutri, R. M., & Low, F. J. 1995, ApJ, 450, L1
Isobe, T., Feigelson, E. D., & Nelson, P. I. 1985, BAAS, 17, 573
Isobe, T., Feigelson, E. D., & Nelson, P. I. 1986, ApJ, 306, 490
Iwasawa, K. 1999, MNRAS, 302, 96
Iwasawa, K., Fabian, A. C., & Ettori, S. 2001, MNRAS, 321, L15
Iwasawa, K., Crawford, C. S., Fabian, A. C., & Wilman, R. J. 2005, MNRAS, 362, L20
Jiménez-Bailón, E., Santos-Lleó, M., Piconcelli, E., et al. 2007, A&A, 461, 917
Kaastra, J. S., & Mewe, R. 1993, A&AS, 97, 443
Kellogg, E., Baldwin, J. R., & Koch, D. 1975, ApJ, 199, 299
Kennicutt, R. C. 1998, ApJ, 498, 541
Kii, T., Williams, O. R., Ohashi, T., et al. 1991, ApJ, 367, 455
Kleinmann, S. G., Hamilton, D., Keel, W. C., et al. 1988, ApJ, 328, 161
Lilly, S. J., Eales, S. A., Gear, W. K. P., et al. 1999, ApJ, 518, 641
Magdziarz, P., & Zdziarski, A. A. 1995, MNRAS, 273, 837
Magorrian, J., Tremaine, S., Richstone, D., et al. 1998, AJ, 115, 2285
Marconi, A., Risaliti, G., Gilli, R., et al. 2004, MNRAS, 351, 169
Mateos, S., Barcons, X., Carrera, F. J., et al. 2005, A&A, 433, 855
McLure, R. J., & Dunlop, J. S. 2002, MNRAS, 331, 795
Mewe, R., Gronenschild, E. H. B. M., & van den Oord, G. H. J. 1985, A&AS, 62, 197
Moshir, M., Kopan, G., Conrow, T., et al. 1990, in IRAS Faint Source Catalogue, version 2.0 (1990)
Mushotzky, R. F. 2004, in Clusters of Galaxies: Probes of Cosmological Structure and Galaxy Evolution, ed. J. S. Mulchaey, A. Dressler, & A. Oemler, 123
Nandra, K., & Pounds, K. A. 1994, MNRAS, 268, 405
Nandra, K., Fabian, A. C., Brandt, W. N., et al. 1995, MNRAS, 276, 1
Ogasaka, Y., Inoue, H., Brandt, W. N., et al. 1997, PASJ, 49, 179
Osterbrock, D. E. 1989, Astrophysics of gaseous nebulae and active galactic nuclei (Mill Valley, CA, University Science Books)
Page, M. J., Mittaz, J. P. D., & Carrera, F. J. 2001, MNRAS, 325, 575
Page, M. J., Davis, S. W., & Salvi, N. J. 2003, MNRAS, 343, 1241
Page, M. J., Stevens, J. A., Ivison, R. J., & Carrera, F. J. 2004, ApJ, 611, L85
Page, M. J., Carrera, F. J., Ebrero, J., Stevens, J. A., & Ivison, R. J. 2007, in Studying Galaxy Evolution with Spitzer and Herschel, ed. V. Charmandaris, D. Rigopoulou, & N. Kylafis
Panessa, F., Bassani, L., Cappi, M., et al. 2006, A&A, 455, 173
Peeters, E., Spoon, H. W. W., & Tielens, A. G. G. M. 2004, ApJ, 613, 986
Persic, M., & Rephaeli, Y. 2002, A&A, 382, 843
Persic, M., Rephaeli, Y., Braito, V., et al. 2004, A&A, 419, 849
Piconcelli, E., Jimenez-Bailón, E., Guainazzi, M., et al. 2005, A&A, 432, 15

Read, A. M., & Ponman, T. J. 2003, A&A, 409, 395
Reeves, J. N., & Turner, M. J. L. 2000, MNRAS, 316, 234
Risaliti, G., & Elvis, M. 2004, A Panchromatic View of AGN, ASSL, 308, Supermassive Black Holes in the Distant Universe), 187
Ross, R. R., & Fabian, A. C. 1993, MNRAS, 261, 74
Rowan-Robinson, M. 2000, MNRAS, 316, 885
Sanders, D. B., & Mirabel, I. F. 1996, ARA&A, 34, 749
Sarazin, C. L. 1986, Rev. Mod. Phys., 58, 1
Saxton, R. D., Barstow, M. A., Turner, M. J. L., et al. 1997, MNRAS, 289, 196
Silverman, J. D., Green, P. J., Barkhouse, W. A., et al. 2005, ApJ, 624, 630
Smail, I., Ivison, R. J., & Blain, A. W. 1997, ApJ, 490, L5
Soifer, B. T., Sanders, D. B., Madore, B. F., et al. 1987, ApJ, 320, 238
Spergel, D. N., Verde, L., Peiris, H. V., et al. 2003, ApJS, 148, 175
Spoon, H. W. W., Armus, L., Cami, J., et al. 2004, ApJS, 154, 184
Stevens, J. A., Page, M. J., Ivison, R. J., et al. 2005, MNRAS, 360, 610
Tran, Q. D., Lutz, D., Genzel, R., et al. 2001, ApJ, 552, 527
Veilleux, S., Kim, D.-C., Sanders, D. B., Mazzarella, J. M., & Soifer, B. T. 1995, ApJS, 98, 171
Veilleux, S., Kim, D.-C., & Sanders, D. B. 1999, ApJ, 522, 113
Veilleux, S., Kim, D.-C., & Sanders, D. B. 2002, ApJS, 143, 315
Verma, A., Rowan-Robinson, M., McMahon, R., & Andreas Efstathiou, A. E. 2002, MNRAS, 335, 574
Véron-Cetty, M.-P., & Véron, P. 2006, A&A, 455, 773
Wang, J., Wei, J. Y., & He, X. T. 2006, ApJ, 638, 106
White, N. E., Swank, J. H., & Holt, S. S. 1983, ApJ, 270, 711
Wilman, R. J., Fabian, A. C., Cutri, R. M., Crawford, C. S., & Brandt, W. N. 1998, MNRAS, 300, L7
Wilman, R. J., Fabian, A. C., Crawford, C. S., & Cutri, R. M. 2003, MNRAS, 338, L19
Yamashita, A., Matsumoto, C., Ishida, M., et al. 1997, ApJ, 486, 763
Yaqoob, T., & Serlemitsos, P. 2005, ApJ, 623, 112
Yun, M. S., & Scoville, N. Z. 1998, ApJ, 507, 774

Online Material

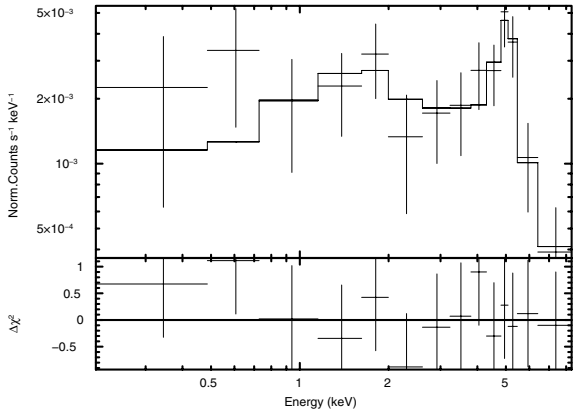

(a) IRAS 00182-7112: PN

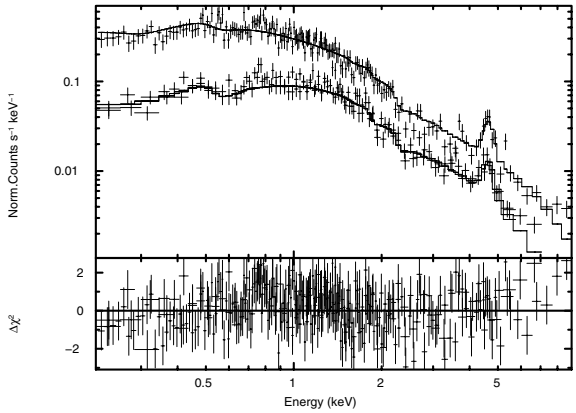

(b) IRAS 09104+4109: PN, MOS1, MOS2

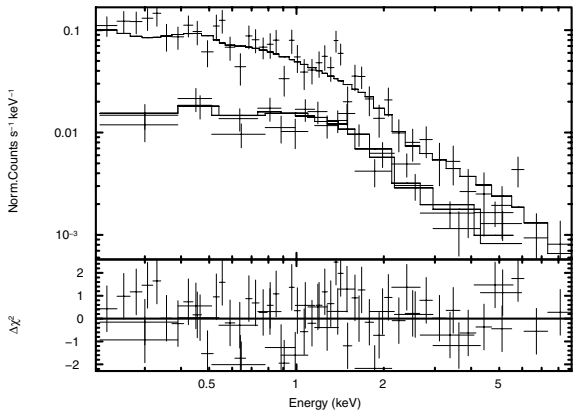

(c) PG 1206+459: PN, MOS1, MOS2

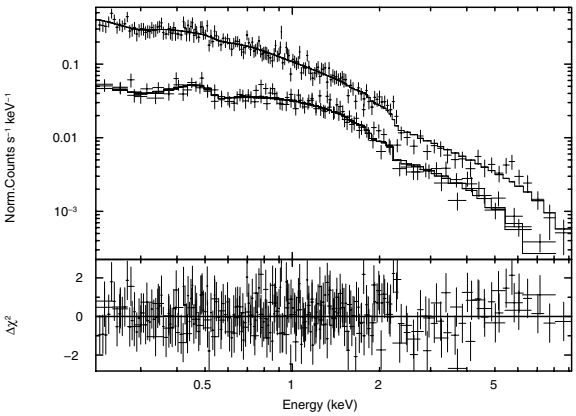

(d) PG 1247+267: PN, MOS1, MOS2

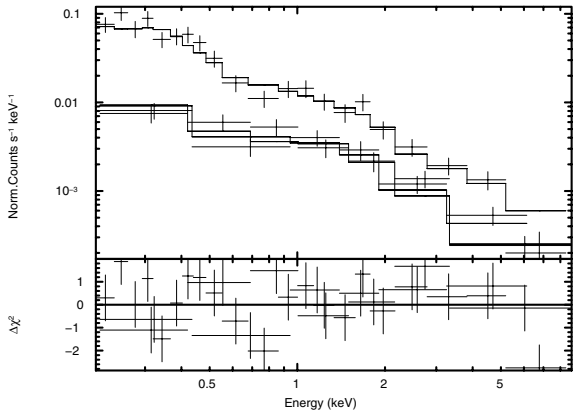

(e) IRAS F12509+3122: PN, MOS1, MOS2

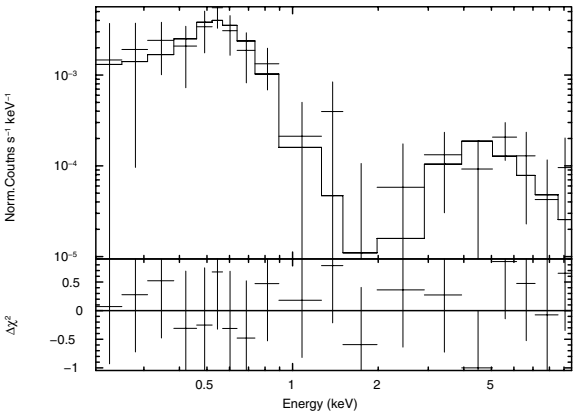

(f) IRAS 12514+1027: PN+MOS1+MOS2

Fig. 1. XMM-*Newton* X-ray spectra and residuals of the detected sources from the HLIRGs sample. The solid line is the best fit model. Continues in next figure.

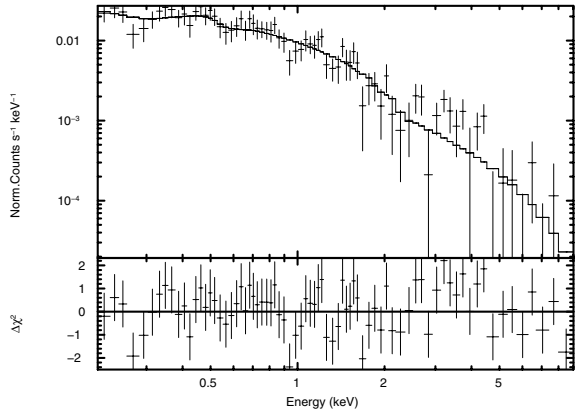

(g) IRAS F14218+3845: PN+MOS1+MOS2 (two observations)

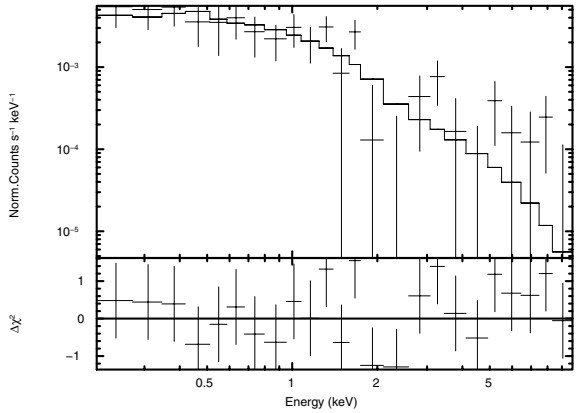

(h) IRAS F15307+3252: PN+MOS1+MOS2

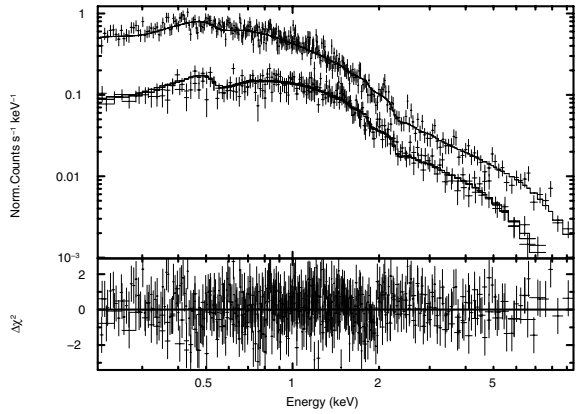

(i) IRAS 16347+7037: PN, MOS1, MOS2

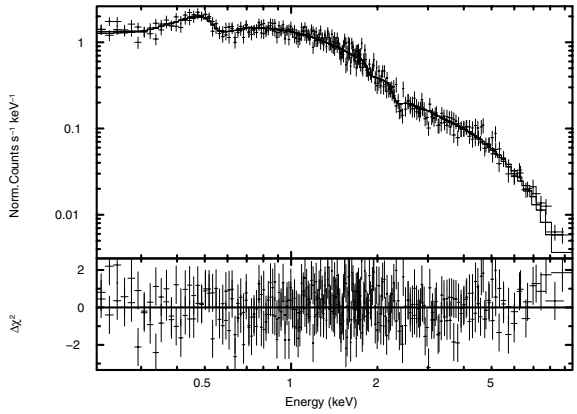

(j) IRAS 18216+6418: MOS1, MOS2

Fig. 1. continued.